International Journal of Advanced Geosciences, 14 (1) (2026) 55-64

International Journal of Advanced Geosciences

Website: www.sciencepubco.com/index.php/IJAG
https://doi.org/10.14419/ag6bv476
Research paper

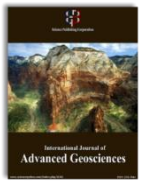

Integrated Spectral Analysis and Source Parameter Imaging (SPI) of High-Resolution Aeromagnetic Data for Basement Depth Estimation in The Yola Arm, Upper Benue Trough, Nigeria

Lucky Peter Kenda [1, 2] *, Adetola Sunday Oniku [2], Bello Yusuf Idi [2], Yohanna Andarawus [3] Sebastian Abraham Sunu [2, 4], Gabriel Joseph Wirdzelii [1]

[1] Department of Physics, Taraba State University, Jalingo, Taraba State, Nigeria
[2] Physics Department, Modibbo Adama University, Yola, Adamawa State, Nigeria
[3] Department of Geology, Federal University of Lafia, Nigeria
[4] Department of Petroleum Chemistry & Physics American University of Nigeria (AUN)
**Corresponding author E-mail: kendalucky1@gmail.com*

Received: April 8, 2026, Accepted: May 17, 2026, Published: May 22, 2026

Abstract

The Yola Arm of the Upper Benue Trough in Nigeria is a geologically complex region with limited subsurface data, hindering a detailed understanding of its basement configuration and sedimentary architecture. This study employs high-resolution aeromagnetic data to estimate basement depths and characterize subsurface structural variations using both spectral analysis and Source Parameter Imaging (SPI). The aeromagnetic data were processed with standard corrections, Reduction to the Equator (RTE), and regional-residual separation to enhance anomaly interpretation. Spectral analysis of 28 overlapping blocks identified shallow magnetic sources ranging from 0.10 to 0.95 km (average 0.55 km), typically associated with intrusive bodies or mineralized zones, and deeper sources from 0.70 to 3.20 km (average 1.95 km), likely corresponding to structural depressions and variable sediment thickness. SPI results revealed depths from 160 m to over 3,400 m, highlighting significant basement heterogeneity. Depth variations are consistent with fault-controlled horst-and-graben structures, reflecting rift-related tectonics and differential sediment accumulation. Integration of the spectral and SPI methods provides a reliable characterization of basement morphology, indicating basement uplifts in the northwestern and central areas and deeper sub-basins in the southeastern parts.

Keywords: *Aeromagnetic Data; Spectral Analysis; Source Parameter Imaging (SPI); Basement Depth; Yola Arm.*

1. Introduction

The Upper Benue Trough, including the Yola Arm, has attracted considerable geological and geophysical interest due to its complex tectonic evolution as part of the West and Central African Rift System and its structurally controlled sedimentary architecture typical of rift basins [1 - 3] However, direct subsurface information from drilling remains sparse across large portions of the basin, limiting detailed understanding of its basement configuration and sedimentary architecture. As a result, potential field methods, especially aeromagnetic surveys, have become an effective and cost-efficient tool for regional subsurface mapping. [4], [5]. Information on basement morphology and sediment thickness is essential for understanding basin evolution and tectonic setting in sedimentary basins. [4], [6 - 8].

Magnetic surveys explore subsurface geology by detecting anomalies in the Earth's magnetic field caused by differences in the magnetic properties of underlying rocks.[8 - 10]. These variations are widely used to delineate faults, fractures, intrusions, and basement relief, as well as to estimate the depth to magnetic sources. [7], [11], [12]. Advances in data interpretation have led to the development of several quantitative techniques, including spectral analysis, Source Parameter Imaging (SPI), Euler deconvolution, and inversion-based methods, which enhance the reliability of subsurface characterization. [12], [13]. Among these techniques, spectral analysis is a widely applied frequency-domain approach for estimating average depths to ensembles of magnetic sources based on the energy spectrum of aeromagnetic data [14 - 17]. In contrast, Source Parameter Imaging (SPI) provides spatially continuous depth estimates derived from local wavenumber analysis, allowing rapid mapping of magnetic source depths across a study area. [18], [19]. The combination of spectral analysis and SPI provides complementary advantages, where spectral methods yield regional depth averages while SPI offers higher spatial resolution of depth variations.

Previous geophysical investigations in the Benue Trough have applied aeromagnetic methods to delineate basement structure and sedimentary architecture, revealing depth variations consistent with rift-related tectonic processes [20], [21]. However, detailed integrated

applications of spectral analysis and SPI focused on the Yola Arm remain limited. This study, therefore, applies both methods to high-resolution aeromagnetic data to estimate basement depth and characterize subsurface structural variations within the study area.

2. Location and Geological Setting of The Study Area

The area of study (Fig.1) lies within the Upper Benue Trough between latitudes 9°00′00″ to 10°00′00″ N and longitudes 11°30′00″ to 13°00′00″ E, covering roughly 18,481.5 km², and is geologically characterized by a complex assemblage of Precambrian Basement Complex rocks overlain by Cretaceous sedimentary successions. The crystalline basement is composed predominantly of gneiss, migmatite, augen gneiss, granite gneiss, hornblende granite, and coarse- to medium-grained granitic intrusions, which represent metamorphosed metasedimentary sequences and older granitoids that have undergone intense deformation, metamorphism, and magmatic reworking during Precambrian tectonothermal events [22 - 24]. The augen gneisses within the basement complex typically display characteristic eye-shaped feldspar porphyroclasts produced by strong ductile deformation during regional metamorphism. [24], [25].

These Precambrian basement rocks are unconformably overlain by Albian-Cretaceous sedimentary units of the Benue Trough, notably Bima Sandstone, Yolde Formation, and Dukul Formation, together with associated shale, limestone, and calcareous sandstone facies. [22], [23], [26]. The Bima Sandstone forms the basal sedimentary unit of the Benue Trough and rests directly on the crystalline basement. It is widely interpreted as being derived largely from granitic source terrains and commonly exhibits feldspathic lower beds that grade upward into less feldspathic sandstones. [22], [23].

The lower parts of the sedimentary succession in the Yola Arm are dominated by calcareous sandstone and shale, indicating a transition from continental fluvial depositional environments to shallow marine conditions. Localized limestone interbeds near the base mark the Yolde Formation, which signifies the onset of marine transgression into the basin.[22], [26]. Overlying units such as the Dukul Formation reflect continued marine influence and progressive basin subsidence during the Cretaceous.[26].

In more recent times, Quaternary alluvial deposits occur along major drainage channels within the Yola Arm. These deposits consist of unconsolidated sands, silts, and clays formed through weathering and erosion of both Precambrian basement rocks and the overlying Cretaceous sedimentary formations. [22].

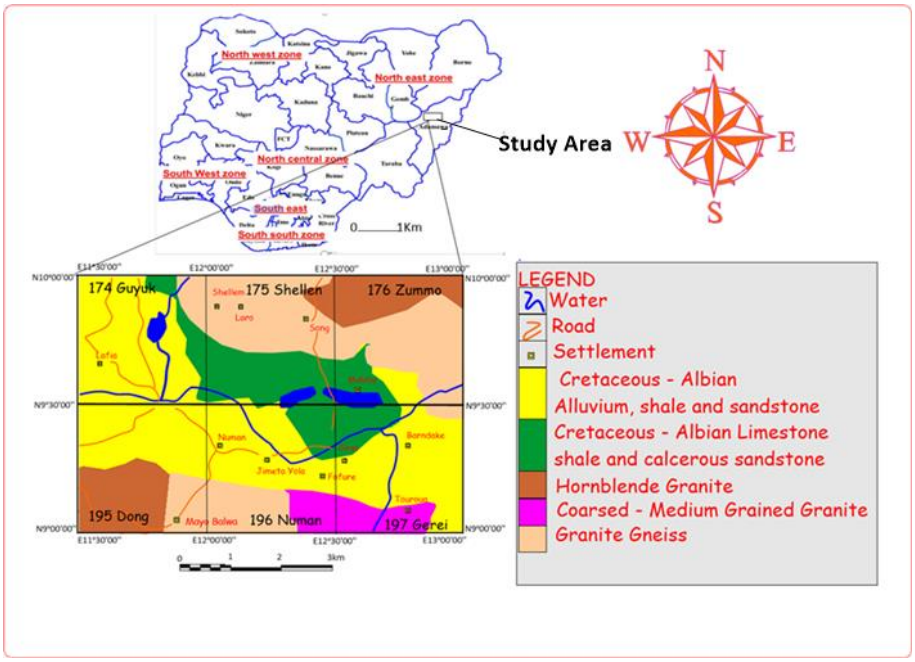

Fig. 1: Geological Map of the Study Area: Map Showing Lithologies Including Cretaceous-Albian Sediments, Hornblende Granite, Granite Gneiss, and Coarse-to-Medium Grained Granite. Water Bodies, Roads, and Settlements Are Indicated. The Inset Shows the Study Area Location within Nigeria.

3. Materials and Methods

This study utilized high-resolution aeromagnetic data covering sheets 174 (Guyuk), 175 (Shelleng), 176 (Zummo), 195 (Dong), 196 (Numan), and 197 (Gerei), obtained from the Nigerian Geological Survey Agency (NGSA). The data were acquired between 2003 and 2009 by Fugro Airborne Surveys using airborne magnetic surveying techniques. Processing and interpretation were carried out using Geosoft Oasis Montaj™ 8.4 software. Standard preprocessing corrections were applied during data acquisition, including compensation for diurnal variations and removal of the Earth's main magnetic field using the Definitive Geomagnetic Reference Field (DGRF-2005), ensuring that the dataset represents only crustal magnetic anomalies [8], [13]. To enhance anomaly interpretation, the data were further processed using Reduction to the Equator (RTE) and regional-residual separation techniques. Since the study area is located in a low magnetic latitude region, RTE was applied to correct for the effects of magnetic inclination and declination, thereby repositioning anomalies closer to their causative sources and reducing asymmetry in the magnetic field [27]. The transformation was implemented using a two-dimensional Fast Fourier Transform (2D-FFT), assuming an inclination of -5.5° and a declination of -1.5°. Following preprocessing, two complementary depth estimation techniques, spectral analysis and Source Parameter Imaging (SPI), were applied to characterize the magnetic basement. For spectral analysis, the residual magnetic intensity (RMI) map was subdivided into 28 overlapping square blocks to capture spatial variations in basement depth. For each block, radial power spectrum analysis was carried out using the MAGMAP filtering module in Oasis Montaj, generating plots of spectral energy versus frequency (cycles/km). The resulting spectral outputs were exported to MATLAB, where logarithmic plots of spectral energy against frequency were generated. These plots revealed

two dominant linear segments corresponding to shallow (high-frequency) and deep (low-frequency) magnetic sources. The slopes of these segments were extracted and used to compute depths to magnetic sources based on standard spectral depth relationships.
In addition, Source Parameter Imaging (SPI) was applied to provide spatially continuous depth estimates across the study area. SPI is based on local wavenumber analysis of the magnetic field and allows automatic estimation of depth to magnetic sources from gridded aeromagnetic data. The Residual Magnetic intensity data were processed within Oasis Montaj using the SPI module, which computes the local wavenumber from first and second horizontal and vertical derivatives of the magnetic field. Depth estimates were then generated automatically for each grid cell, producing a continuous depth-to-source map. This approach enables rapid identification of both shallow and deep magnetic sources and complements the block-based spectral analysis by providing higher spatial resolution of structural variations. The integration of spectral analysis and SPI allowed for both regional averaging of depth estimates and detailed spatial mapping of basement relief, thereby improving the reliability and geological interpretation of subsurface structures within the study area.

3.1. Depth to magnetic sources estimation

Basement depth estimation in this study was performed using the radially averaged power spectrum method. [16], [17]. The analysis was conducted on the residual magnetic field, which enhances anomalies associated with subsurface magnetic sources while suppressing regional trends. The method is based on the principle that the spectral content of magnetic anomalies is directly related to the depth of their causative bodies. To utilize this relationship, the magnetic data were transformed from the spatial domain into the wave-number domain using the Fourier transform, allowing the distribution of anomaly energy with respect to frequency to be examined.
For a simple magnetic source, the amplitude spectrum decays exponentially with increasing wave number:

$$F(\omega) = \exp^{-h\omega} \tag{1}$$

Where F(ω) is the amplitude spectrum, ω is the angular wave number (rad/km), and h is the depth to the top of the magnetic source (km).
For a source with finite thickness (e.g., a prism), the spectral response incorporates contributions from both the upper and lower boundaries:

$$F(\omega) = \exp^{h_t\omega}\text{-}\exp^{h_b\omega} \tag{2}$$

Where h_t and h_b represent the depths to the top and bottom of the source, respectively. These expressions indicate that deep-seated sources dominate the low wave-number region, whereas shallow sources contribute to higher wave numbers.
The energy spectrum, E(k), is proportional to the square of the amplitude spectrum:

$$E(K) = |F(K)|^2 \tag{3}$$

Taking the natural logarithm gives:

$$\ln E(k) = -2hk + C \tag{4}$$

Where k is the wave number (cycles/km), h is the average depth to the source ensemble, and C is a constant.
This linear relationship forms the basis of spectral depth estimation. The slope m of the straight-line segment on a plot of $\ln E(k)$ versus k is:

$$m = -2h \tag{5}$$

The natural logarithm formulation was adopted in this study; hence, depth was estimated from the slope using:

$$h = -\frac{m}{2} \tag{6}$$

In practice, two distinct linear segments are commonly observed, corresponding to shallow and deep magnetic sources. Their depths are estimated using:

$$Z_1 = -\frac{m_1}{2} \tag{7}$$

$$Z_2 = -\frac{m_2}{2} \tag{8}$$

Where m_1 and m_2 are the slopes of the respective segments, Z_1 and Z_2 represent shallow and deep source depths.
The radially averaged power spectrum was computed for selected data windows. The linear segments were identified from the low- and high-wave-number portions of the log-spectrum, representing deep and shallow source ensembles, respectively, and their slopes were computed using least-squares linear regression. The resulting depth estimates Z_1 and Z_2 were interpolated and contoured using Surfer 29 to produce maps of shallow and deep basement configurations.

3.2. Source parameter imaging (SPI)

To validate the basement depths derived from spectral analysis, the Source Parameter Imaging (SPI) technique was applied as an independent validation method. SPI is particularly effective for aeromagnetic data in low-latitude regions because its depth solutions are not significantly influenced by magnetic inclination, declination, or remanent effects [19], [28].
The method is based on the analytical signal, which combines horizontal and vertical derivatives of the magnetic field:

$$A(x, z) = \frac{\partial B(x,z)}{\partial x} - j\frac{\partial B(x,z)}{\partial z} \tag{9}$$

Where B(x,z) represents the total magnetic intensity, and x and z denote the horizontal and vertical coordinates, respectively. The amplitude of this signal enhances anomaly boundaries, while its phase contains information related to source geometry.
This complex quantity can also be represented in exponential (polar) form:

$$A\,(x,z) = /A/\ exp\,(j\theta) \tag{10}$$

Where $|A| = \sqrt{\left(\frac{\partial B}{\partial x}\right)^2 + \left(\frac{\partial B}{\partial y}\right)^2}$ corresponds to the magnitude of the analytical signal, while θ defines its phase angle, given by $\theta = tan^{-}\left[\frac{\partial T/\partial z}{\partial T/\partial x}\right]$.
To further characterize the spatial variation of the magnetic field, Thurston and Smith (1997) introduced the concept of local frequency f, which describes how rapidly the phase changes along the horizontal direction:

$$f = \frac{1}{2\pi}\frac{\partial}{\partial x} tan^{-1}\left[\frac{\partial T/\partial z}{\partial T/\partial x}\right] \tag{11}$$

Depth estimation in SPI relies on the local wavenumber K, derived from the spatial variation of the analytical signal phase: $K = 2\pi f$

$$K = \frac{1}{|A|^2}\left(\frac{\partial^2 B}{\partial x \partial z}\frac{\partial B}{\partial x} - \frac{\partial^2 B}{\partial x^2}\frac{\partial B}{\partial z}\right) \tag{12}$$

The depth of the magnetic source was obtained from the inverse of the maximum local wavenumber:

$$h = \frac{1}{K_{Max}} \tag{13}$$

Thus, zones characterized by high wavenumber values correspond to shallow magnetic sources, whereas lower values indicate deeper basement configurations. [19].

4. Results and Discussion

The TMI map (Fig.2) displays variation in magnetic intensity, with anomalies ranging from 31178.39 nT to 31355.91nT, highlighting both high and low magnetic intensity zones throughout the study region. These variations in magnetic signals are influenced by factors such as rock susceptibility, depth to the magnetic source, structural strike, and remnant magnetization.[29], [30]. High-intensity zones, marked in red, likely correspond to regions with dense, magnetically strong rocks, such as iron-rich formations or mafic intrusions.[4], [31], while low-intensity zones (blue and purple) suggest areas with less magnetic material, possibly sedimentary rocks or weathered formations[31].

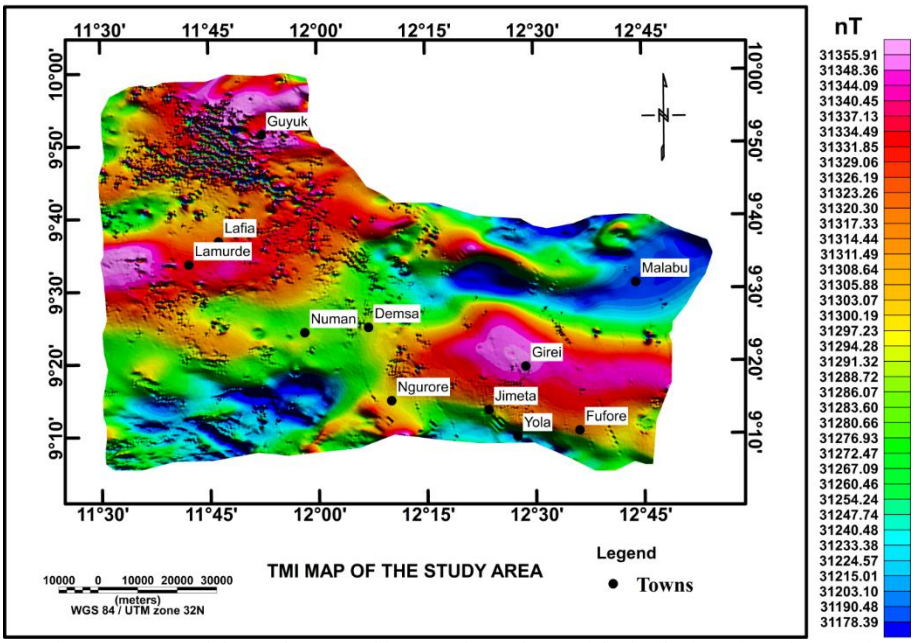

Fig. 2: Total Magnetic Intensity (TMI) Map of the Study Area: This Map Shows the Spatial Distribution of Total Magnetic Intensity Across the Study Area. Towns Are Marked with Black Dots, and the Colour Gradient Indicates Variations in Magnetic Field Strength (nT). Latitude And Longitude Coordinates, A Scale Bar, A North Arrow, and A Legend Are Included for Reference.

The RTE map (Fig.3), which accounts for the Earth's magnetic field inclination, shows anomalies within the intensity range of 31185.80 nT to 31349.46 nT. By reducing the effects of inclination, the RTE map provides a clearer picture of the underlying geological structures. The anomalies in this map are more aligned, with linear patterns often corresponding to tectonic features such as fault zones or mineralized zones.

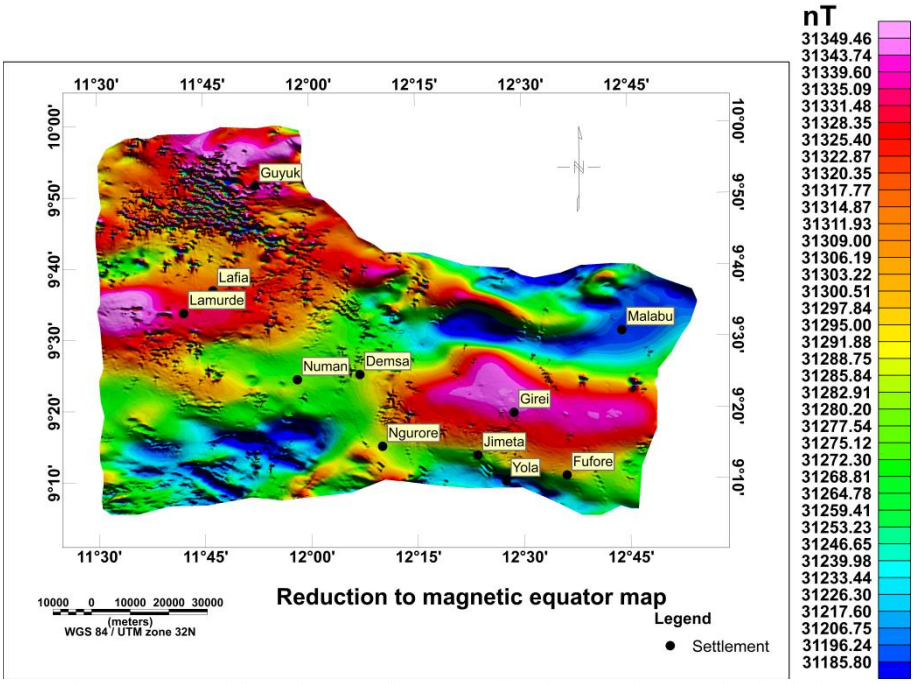

Fig. 3: Reduction to the Magnetic Equator Map of the Study Area: This Map Displays the Magnetic Anomaly Distribution After Reduction to the Magnetic Equator. Coloured Gradients Represent Variations in Magnetic Intensity (nT), While Black Dots Indicate Settlements. The Map Includes Latitude and Longitude Coordinates, A North Arrow, A Scale Bar, and A Legend for Reference.

The structural trends in the RTE map further emphasize the role of regional tectonic forces, particularly the NW-SE, N-S, and E-W orientations, in shaping the magnetic anomalies.

The Residual Magnetic Intensity (RMI) map (Fig.4), which isolates local anomalies by removing the regional magnetic trend, shows a range of intensities from -76.33 nT to 100.84 nT. Positive residual anomalies indicate strong localized magnetic sources, such as intrusive bodies or mineralized zones, while negative residual anomalies suggest weak or deeper sources, possibly related to sedimentary rocks or deeply buried structures. [32], [33]. The sharp contrasts between high and low residual intensities highlight fault zones or geological contacts, while the more diffuse anomalies suggest areas of overlapping or complex magnetic sources.[34], [35].

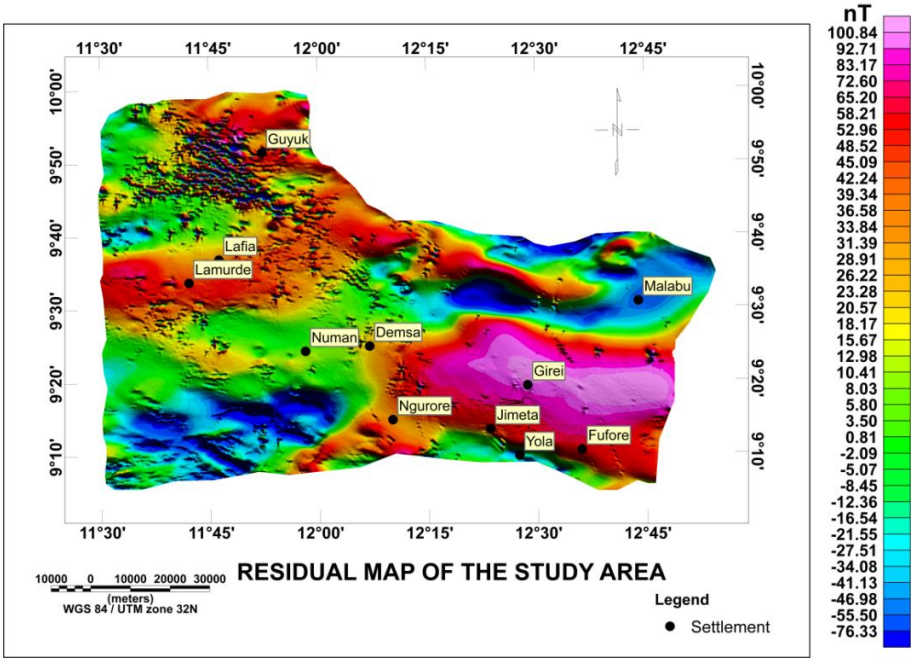

Fig. 4: Residual Magnetic Intensity Map of the Study Area: This Map Shows the Residual Magnetic Anomalies After Regional Field Removal. Colour Gradients Indicate Variations in Residual Magnetic Intensity (nT), While Black Dots Represent Settlements. The Map Includes Latitude and Longitude Coordinates, A Scale Bar, A North Arrow, and A Legend for Reference.

The Spectral analysis revealed two distinct depth categories corresponding to shallow and deep magnetic sources, reflecting subsurface structural variations, with high-frequency components associated with shallow sources and low-frequency components linked to deeper sources, consistent with [8], [16]. The shallow magnetic sources range from 0.10 to 0.95 km, averaging 0.55 km, where deeper shallow anomalies (0.70-0.95 km) are interpreted as near-surface intrusions or structurally controlled features, moderately shallow sources (0.35-0.60 km) are associated with faults, fractures, or layered sedimentary units, and very shallow sources (0.10-0.35 km) reflect near-surface magnetic variations [7], [13]. The deeper magnetic sources range from 0.70 to 3.20 km, with an average depth of 1.95 km, representing

the magnetic basement configuration, where depths of 2.70-3.20 km indicate basement depressions or sub-basins, 1.70-2.45 km correspond to faulted or dipping basement blocks, and 0.70-1.50 km suggest uplifted basement or intrusive features [20], [36].

Spatial depth variations observed in spectral plots (Fig.5), contour maps (Fig.6 and Fig.7), and 3D modelling (Fig.8) indicate a structurally complex and heterogeneous basement morphology, with undulating surfaces reflecting faults, folds, and block faulting associated with tectonic deformation. [37], [38]. These variations are consistent with a fault-controlled rift system typical of the Benue Trough, where alternating shallow and deep basement zones reflect horst and graben architecture formed by extensional tectonics and differential subsidence. [20], [37], [39]. The deeper zones represent fault-controlled structural depressions that influenced sediment accumulation, while shallower zones correspond to basement uplifts or structural highs, indicating reduced sediment thickness and possible uplift or inversion. [1]. The alignment of these depth variations further suggests regional structural trends linked to known tectonic lineaments that contributed to basin evolution, segmentation, and deformation. [38], [39]. Graphs showing the logarithm of spectral energy plotted against frequency (cycles/km) for blocks 1, 2, 8, 9, 10, 11, 27, and 28 are shown in Fig.5.

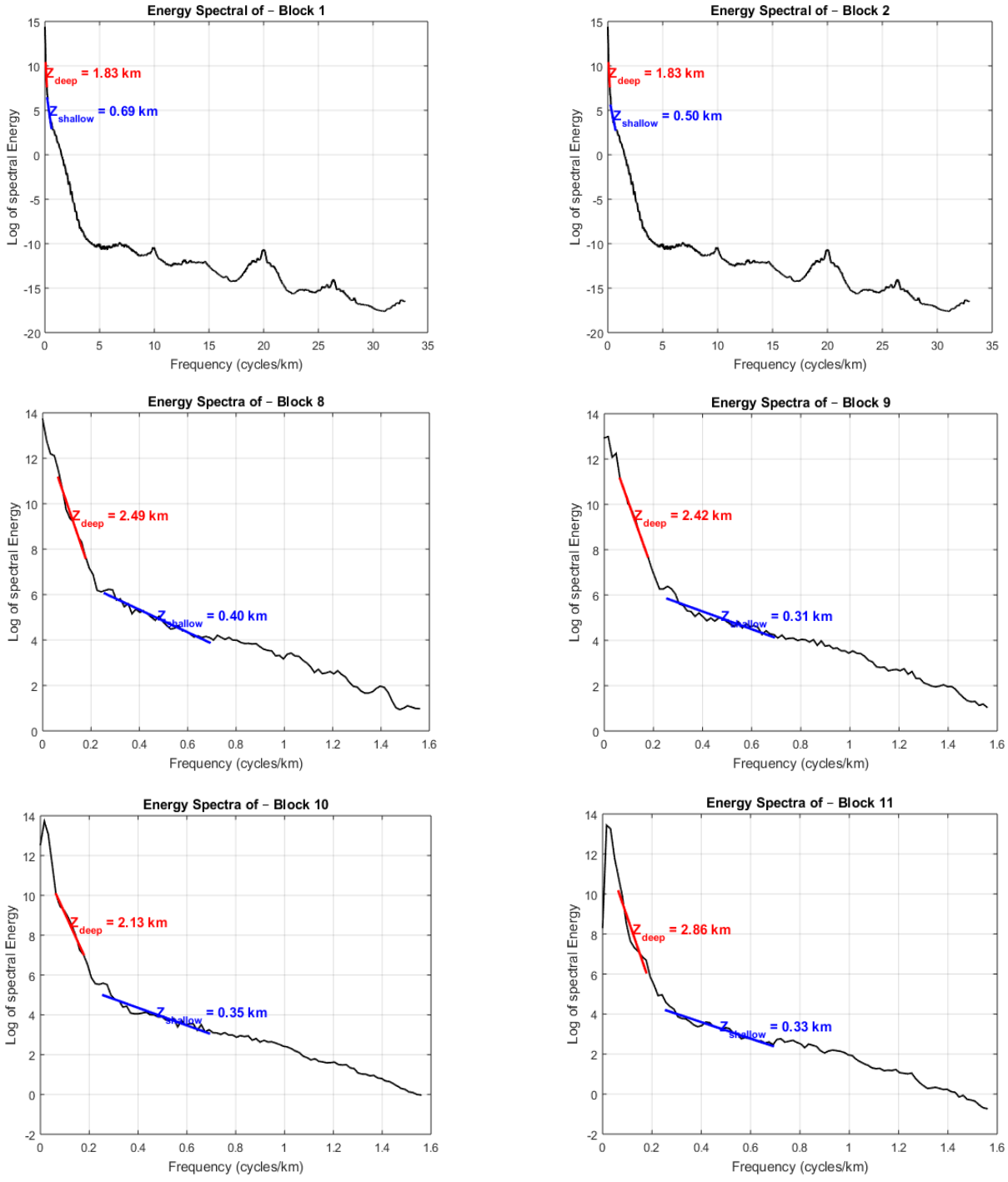

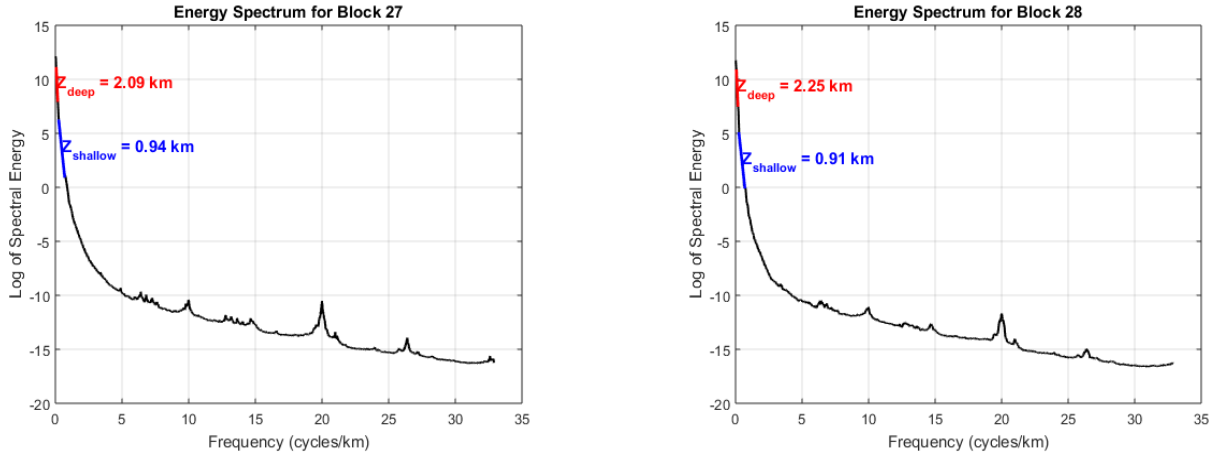

Fig. 5: Plots of the Logarithm of Spectral Energy Versus Frequency (Cycles/Km): the Plots Show the Logarithm of Spectral Energy Versus Frequency (Cycles/Km) for Blocks 1, 2,8,9,10,11, 27, and 28. Shallow and Deep Source Depths Are Estimated From The High- and Low-Frequency Slopes of the Spectrum, Respectively, with Shallow Sources Indicated in Blue and Deep Sources in Red.

Table 1: The Calculated Depths for Both Deep and Shallow Magnetic Sources for Blocks 1-28

S/No	Spectral Block	Longitude(°)	Latitude(°)	Deep Sources(D1)Km	Shallow Sources(D2)Km
1	Block 1	11.6	9.2	1.83	0.69
2	Block 2	11.8	9.2	1.83	0.50
3	Block 3	12	9.2	2.04	0.40
4	Block 4	12.2	9.2	2.75	0.41
5	Block 5	12.4	9.2	2.63	0.43
6	Block 6	12.6	9.2	2.80	0.23
7	Block 7	12.8	9.2	2.71	0.14
8	Block 8	11.6	9.4	2.49	0.40
9	Block 9	11.8	9.4	2.42	0.31
10	Block 10	12	9.4	2.13	0.35
11	Block 11	12.2	9.4	2.86	0.33
12	Block 12	12.4	9.4	3.26	0.30
13	Block 13	12.6	9.4	2.98	0.20
14	Block 14	12.8	9.4	2.45	0.17
15	Block 15	11.6	9.6	2.25	0.23
16	Block 16	11.8	9.6	1.11	0.25
17	Block 17	12	9.6	1.49	0.32
18	Block 18	12.2	9.6	2.84	0.28
19	Block 19	12.4	9.6	2.99	0.40
20	Block 20	12.6	9.6	2.84	0.75
21	Block 21	12.8	9.6	2.66	0.88
22	Block 22	11.6	9.8	2.66	0.88
23	Block 23	11.8	9.8	0.83	0.39
24	Block 24	12	9.8	1.20	0.57
25	Block 25	12.2	9.8	2.33	0.30
26	Block 26	12.4	9.8	2.80	0.23
27	Block 27	12.6	9.8	2.09	0.94
28	Block 28	12.8	9.8	2.25	0.91

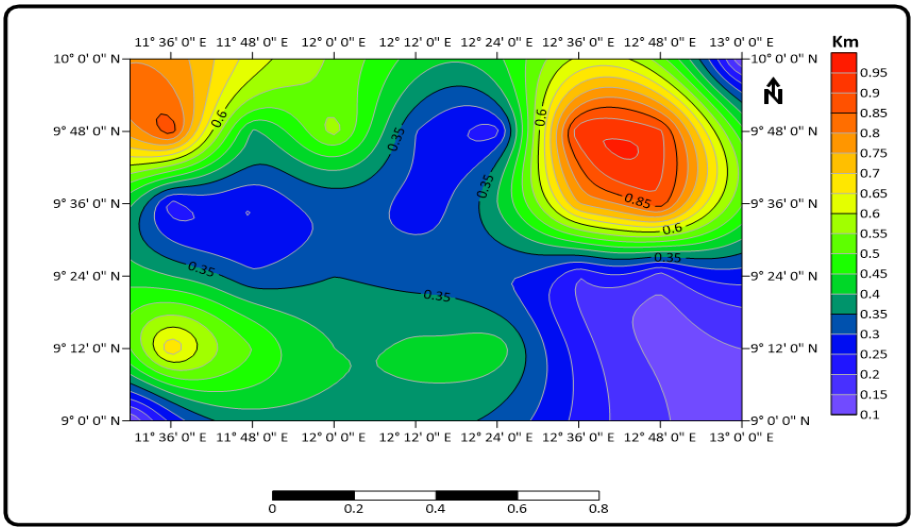

Fig. 6: Depth to Shallow Magnetic Sources Map of the Study Area: Contour Map Showing Estimated Depths to Shallow Magnetic Sources Across the Study Area. Depths (Km) Are Represented by Colour Gradients from 0.1 Km (Purple) To 0.95 Km (Red). Latitude and Longitude Coordinates, A Scale Bar, and A North Arrow Are Included for Spatial Reference.

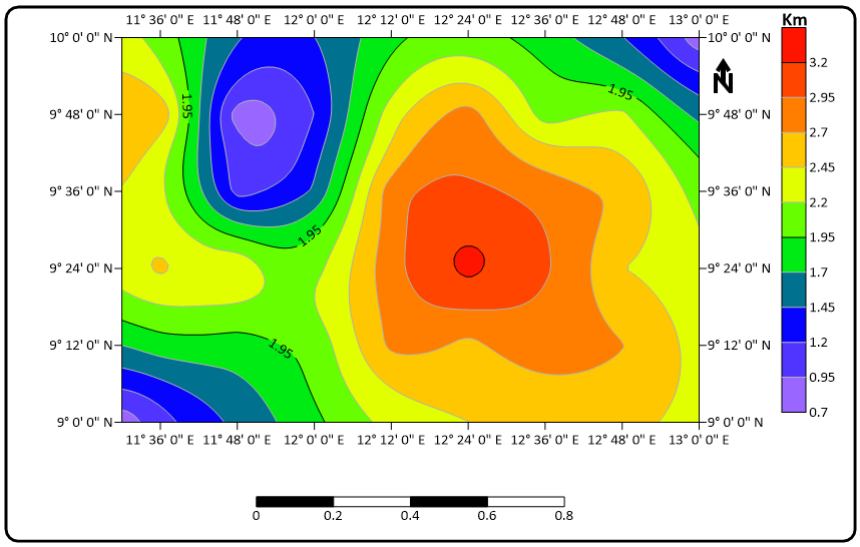

Fig. 7: Depth to Deeper Magnetic Sources Map of the Study Area: Contour Map Showing Estimated Depths to Shallow Magnetic Sources Across the Study Area. Depths (Km) Are Represented by Colour Gradients from 0.7 Km (Purple) to 3.2 Km (Red). Latitude and Longitude Coordinates, A Scale Bar, and A North Arrow Are Included for Spatial Reference.

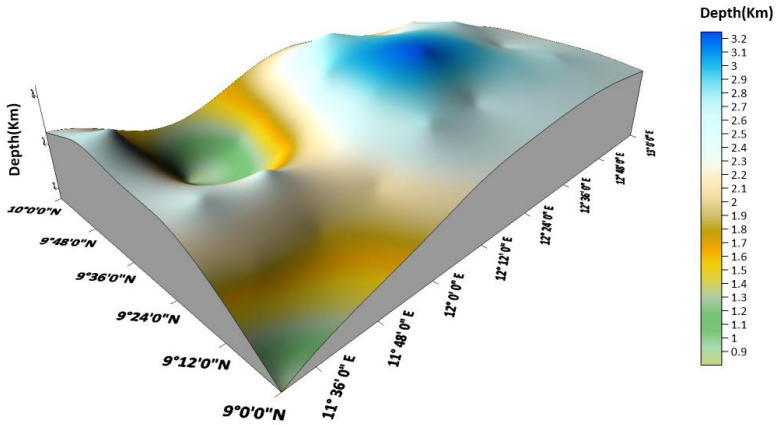

Fig. 8: 3-D Surface Model of Deeper Magnetic Source Depth of the Study Area: Three-Dimensional Surface Showing the Estimated Depths to Deeper Magnetic Sources Across the Study Area. Depths (Km) Are Represented by A Colour Gradient from 0.9 Km (Green) to 3.2 Km (Blue). Latitude and Longitude Coordinates Are Indicated Along the Axes for Spatial Reference.

The Source Parameter Imagery depth map (Fig.9) reveals spatial variation in depths to magnetic sources ranging from approximately 160 m to over 3400 m, indicating significant basement heterogeneity within the study area. This range is consistent with depths typically resolved using SPI techniques in sedimentary basins.[19]. Shallow depths (160-800 m), observed mainly in the northwestern and parts of the central area, suggest basement uplift or thin sedimentary cover. Such shallow magnetic sources are commonly associated with basement highs or near-surface intrusions. [40]. Intermediate depths (800-1700 m) dominate the central region and represent transitional zones with moderate sediment thickness, reflecting relatively stable structural blocks. Deeper sources (1700-3400 m), concentrated in the eastern and southeastern sectors, indicate basement depressions or sub-basins associated with thicker sediment accumulation.

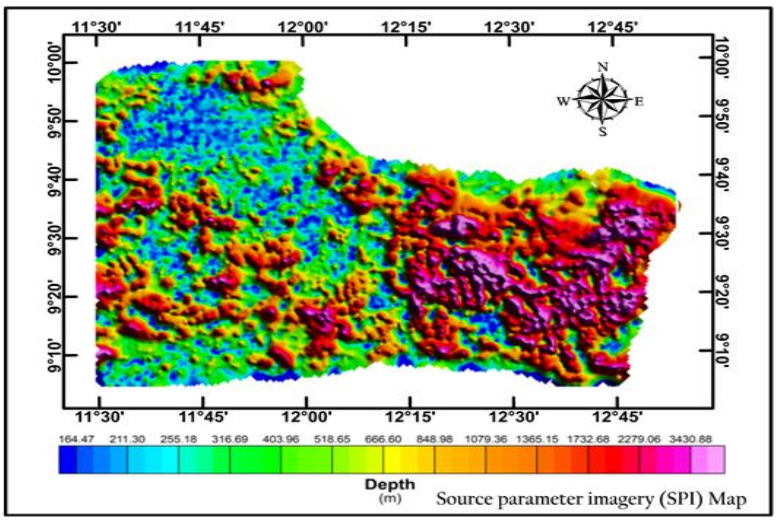

Fig. 9: Source Parameter Imagery Map of the Study Area: This Map Represents Subsurface Magnetic Source Depths Estimated Using Source Parameter Imagery (SPI). Depths (m) Are Shown with A Colour Gradient from Shallow (164 m, Blue) to Deep (3,440 m, Pink). The Map Includes Latitude and Longitude Coordinates, A North Arrow, and A Colour Scale for Reference.

These deeper zones are typically linked to fault-controlled subsidence and rift-related basin development, as documented for the Benue Trough. [20]. Sharp lateral depth contrasts imply the presence of faults or structural discontinuities, reflecting a basement architecture characterized by uplifted and down-faulted blocks (horst-graben systems), a structural style widely reported in rift environments. [37]. The basement depths obtained in this study from spectral analysis (0.10-3.20 km) and SPI (0.16-3.40 km) are consistent with previous estimates in the Upper Benue Trough, which generally range from about 0.26 km to over 4.3 km. [21], [41], [42]. Earlier studies similarly report shallow sources around 0.5-1.5 km and deeper basement levels between 1.5 km and 3.5 km, with thicker sediment accumulation in structurally deeper parts of the basin, particularly toward the southeastern region. [14]. Minor differences in depth values may result from variations in data resolution, methodological approaches, spectral window selection, and interpretation techniques, with SPI offering improved resolution of shallow structures.

5. Conclusion

This study demonstrates the applicability of spectral analysis and Source Parameter Imaging (SPI) for characterizing basement depth and structural variations in the Yola Arm of the Upper Benue Trough. The results indicate a heterogeneous basement, with shallow magnetic sources (0.10-0.95 km) likely corresponding to basement highs or near-surface intrusions, and deeper sources (0.70-3.20 km) associated with structural depressions and thicker sedimentary cover. Depth estimates from both methods are generally consistent, although minor discrepancies reflect methodological differences, data resolution, and spectral window selection, highlighting inherent uncertainties in geophysical depth estimation. The observed basement morphology exhibits features consistent with horst and graben structures typical of rift-related tectonics, suggesting complex structural control on sediment distribution. While the results provide valuable regional insights, the study is limited by the spatial resolution of the aeromagnetic data and the reliance on indirect geophysical interpretations. Hence, these findings should be considered as a preliminary characterization of basement architecture, forming a basis for further detailed geophysical investigations in the region.

6. Conflict of Interest

The authors declare no conflict of interest.

Acknowledgement

The authors gratefully acknowledge the Nigerian Geological Survey Agency (NGSA) for providing the aeromagnetic dataset used in this study. Special thanks to Prof. Adetola Sunday Oniku and Prof. Bello Yusuf Idi for guidance and supervision of this work. The authors also sincerely appreciate the reviewers for their constructive comments and valuable suggestions, which have significantly improved the quality of this manuscript.

References

[1] J. Benkhelil, "The origin and evolution of the Cretaceous Benue Trough (Nigeria)," *J. Afr. Earth Sci. Middle East*, vol. 8, no. 2–4, pp. 251–282, 1989. https://doi.org/10.1016/S0899-5362(89)80028-4.

[2] M. Guiraud, "Tectono-sedimentary framework of the early Cretaceous continental Bima formation (upper Benue Trough, NE Nigeria)," *J. Afr. Earth Sci. Middle East*, vol. 10, no. 1–2, pp. 341–353, 1990. https://doi.org/10.1016/0899-5362(90)90065-M.

[3] J. K. Ogunmola, E. A. Ayolabi, and S. B. Olobaniyi, "Structural-depth analysis of the Yola Arm of the Upper Benue Trough of Nigeria using high-resolution aeromagnetic data," *J. Afr. Earth Sci.*, vol. 124, pp. 32–43, 2016. https://doi.org/10.1016/j.jafrearsci.2016.09.008.

[4] G. B. Gladman, C. N. Nwankwo, and G. O. Emujakporue, "Structural Mapping And Sedimentary Thickness Determination of Bornu Basin Using Source Parameter Imaging Technique," *Int. J. Innov. Environ. Stud. Res.*, vol. 10, no. 1, pp. 103–114, 2022. https://www.seahipublications.org/wp-content/uploads/2024/12/IJIESR-M-9-2022.pdf.

[5] H. Saibi, M. Azizi, and S. Mogren, "Structural Investigations of Afghanistan Deduced from Remote Sensing and Potential Field Data," *Acta Geophys.*, vol. 64, no. 4, pp. 978–1003, Aug. 2016, doi: 10.1515/acgeo-2016-0046. https://doi.org/ 10.1515/acgeo-2016-0046.

[6] P. O. Eke, R. Ombu, and I. N. Onyeche, "Sedimentary thickness and basement depths of eastern Niger delta, Nigeria, from aeromagnetic data and implications for hydrocarbon prospects," *World J. Adv. Eng. Technol. Sci.*, vol. 7, no. 02, pp. 255–261, 2022. https://doi.org/10.30574/wjaets.2022.7.2.0171.

[7] P. Kearey, M. Brooks, and I. Hill, *An introduction to geophysical exploration*, vol. 4. John Wiley & Sons, 2002.

[8] W. M. Telford, L. P. Geldart, and R. E. Sheriff, *Applied geophysics*. Cambridge University Press, 1990. https://doi.org/10.1017/CBO9781139167932.

[9] A. Abubakara, O. K. Likkason, M. A. Sadiq, S. Ali, and A. E. Moses, "Subsurface investigation of geological structures from magnetic method in parts of Kangiwa Gwandu Formation, northwestern, Nigeria," in *Global Meeting Abstracts*, Society of Exploration Geophysicists, 2021, pp. 336–341. https://doi.org/10.1190/iceg2021-085.1.

[10] G. Emujakporue, C. C. Ofoha, and I. Kiani, "Investigation into the basement morphology and tectonic lineament using aeromagnetic anomalies of Parts of Sokoto Basin, North Western, Nigeria," *Egypt. J. Pet.*, vol. 27, no. 4, pp. 671–681, 2018. https://doi.org/10.1016/j.ejpe.2017.10.003.

[11] P. G. Betts *et al.*, "Geology from aeromagnetic data," *Earth-Sci. Rev.*, vol. 258, p. 104958, 2024. https://doi.org/10.1016/j.earscirev.2024.104958.

[12] W. J. Hinze, R. Von Frese, and A. H. Saad, *Gravity and magnetic exploration: Principles, practices, and applications*. Cambridge University Press, 2013. https://doi.org/10.1017/CBO9780511843129.

[13] C. Reeves, *Aeromagnetic surveys: principles, practice and interpretation*, vol. 155. Geosoft Washington (DC), 2005.

[14] S. Bello, E. E. Udensi, K. Salako, and A. A. Adetona, "Determination of Depth to Magnetic Basement Using Spectral Analysis of Aeromagnetic Data over Biu Plateau Basalt and Yola Sub-basin, North East Nigeria," 2018.

[15] B. K. Bhattacharyya and L.-K. Leu, "Analysis of magnetic anomalies over Yellowstone National Park: Mapping of Curie point isothermal surface for geothermal reconnaissance," *J. Geophys. Res.*, vol. 80, no. 32, pp. 4461–4465, Nov. 1975, doi: 10.1029/JB080i032p04461.

[16] A. Spector and F. S. Grant, "Statistical models for interpreting aeromagnetic data," *Geophysics*, vol. 35, no. 2, pp. 293–302, Apr. 1970, doi: 10.1190/1.1440092.

[17] A. Spector and F. S. Grant, "Statistical models for interpreting aeromagnetic data," *Geophysics*, vol. 50, no. 11, pp. 1951–1960, 1985. http://pascal-francis.inist.fr/vibad/index.php?action=getRecordDetail&idt=8546018.

[18] A. B. Reid, J. M. Allsop, H. Granser, A. t Millett, and I. W. Somerton, "Magnetic interpretation in three dimensions using Euler deconvolution," *Geophysics*, vol. 55, no. 1, pp. 80–91, 1990. https://doi.org/10.1190/1.1442774.

[19] J. B. Thurston and R. S. Smith, "Automatic conversion of magnetic data to depth, dip, and susceptibility contrast using the SPI (TM) method," *Geophysics*, vol. 62, no. 3, pp. 807–813, 1997. https://doi.org/10.1190/1.1444190.
[20] J. D. Fairhead and C. S. Okereke, "A regional gravity study of the West African rift system in Nigeria and Cameroon and its tectonic interpretation," *Tectonophysics*, vol. 143, no. 1–3, pp. 141–159, 1987. https://doi.org/10.1016/0040-1951(87)90084-9.
[21] K. A. Salako and E. E. Udensi, "Spectral depth analysis of upper Benue Trough and Borno Basin, northeast Nigeria using aeromagnetic data," 2013. http://irepo.futminna.edu.ng:8080/jspui/handle/123456789/4286.
[22] N. G. Obaje, *Geology and Mineral Resources of Nigeria*, vol. 120. in Lecture Notes in Earth Sciences, vol. 120. Berlin, Heidelberg: Springer Berlin Heidelberg, 2009. doi: 10.1007/978-3-540-92685-6.
[23] J. D. Carter, "The geology of parts of Adamawa, Bauchi and Bornu Provinces in northeastern Nigeria," *Geol. Surv. Niger. Bull.*, vol. 30, 1963. https://cir.nii.ac.jp/crid/1570854175582044160.
[24] J. B. Wright, D. A. Hastings, W. B. Jones, and H. R. Williams, *Geology and mineral resources of West Africa*, vol. 187. Springer, 1985. https://link.springer.com/book/10.1007/978-94-015-3932-6.
[25] M. A. Rahaman, "Recent advances in the study of the basement complex of Nigeria," *Pre-Cambrian. Geol. Niger*, pp. 11–41, 1988. https://cir.nii.ac.jp/crid/1571135650759008768.
[26] P. Zaborski, F. Ugodulunwa, A. Idornigie, P. Nnabo, and K. Ibe, "Stratigraphy and structure of the Cretaceous Gongola Basin, northeast Nigeria," *Bull. Cent. Rech. Explor.-Prod. Elf-Aquitaine*, vol. 21, no. 1, pp. 153–185, 1997. http://pascal-francis.inist.fr/vibad/index.php?action=getRecordDetail&idt=6246048.
[27] C. C. Okpoli, "High resolution magnetic field signatures over Akure and its Environs, southwestern Nigeria," *Earth Sci Malays*, vol. 3, no. 1, pp. 9–17, 2019. http://doi.org/10.26480/esmy.01.2019.09.17.
[28] R. J. Blakely, *Potential theory in gravity and magnetic applications*. Cambridge University Press, 1996. https://doi.org/10.1017/CBO9780511549816.
[29] O. K. Likkason, "Exploring and using the magnetic methods," *Adv. Geosci. Remote Sens.*, pp. 141–174, 2014. http://dx.doi.org/10.5772/57163.
[30] D. N. Obiora, M. N. Ossai, and E. Okwoli, "A case study of aeromagnetic data interpretation of Nsukka area, Enugu State, Nigeria, for hydrocarbon exploration," *Int. J. Phys. Sci.*, vol. 10, no. 17, pp. 503–519, 2015. http://doi.org/10.5897/IJPS2015.4392.
[31] D. A. Clark, "Magnetic petrophysics and magnetic petrology: aids to geological interpretation of magnetic surveys," *AGSO J Aust Geol Geophys*, vol. 17, no. 2, pp. 83–103, 1997. https://cir.nii.ac.jp/crid/1573105975649656448.
[32] A. A. Akinlalu, "Exploration of iron ore deposits in parts of Kogi State, north-central Nigeria: Analyses from airborne magnetic and ASTER datasets," *Geosystems Geoenvironment*, vol. 4, no. 2, p. 100359, 2025. https://doi.org/10.1016/j.geogeo.2025.100359.
[33] A. A. Akinlalu, G. M. Olayanju, K. A. N. Adiat, and G. O. Omosuyi, "Mineralisation potential assessment using analytical hierarchy process (AHP) modelling technique: A case study of Ilesha schist belt, southwestern Nigeria," *Results Geophys. Sci.*, vol. 7, p. 100026, 2021. https://doi.org/10.1016/j.ringps.2021.100026.
[34] Z. Ahmed, K. M. Lawal, and A. L. Ahmed, "Interpretation of High Resolution Aeromagnetic Data of Part of Southwestern Nigeria for Subsurface Mapping," *Dutse J. Pure Appl. Sci.*, vol. 4, no. 2, pp. 221–235, 2018.
[35] S. Ariyo, J. O. Coker, A. O. Alaka, O. A. Adenuga, and O. O. Bayewu, "Integration Of Magnetic Residuals, Derivatives And Located Euler Deconvolution For Structural And Geologic Mapping Of Parts Of The Precambrian Gneisses Of Ago-Iwoye, Southwestern Nigeria," *Geosci. Eng.*, vol. 66, no. 1, pp. 1–32, 2020. http://gse.vsb.cz/ojs/index.php/GSE/article/view/278/197. https://doi.org/10.35180/gse-2020-0027.
[36] D. S. Parasnis, *Principles of applied geophysics*. Springer Science & Business Media, 2012. Accessed: May 13, 2026.
[37] N. K. Grant, "South Atlantic, Benue Trough, and Gulf of Guinea Cretaceous Triple Junction," *Geol. Soc. Am. Bull.*, vol. 82, no. 8, pp. 2295–2298, 1971. https://doi.org/10.1130/0016-7606(1971)82[2295:SABTAG]2.0.CO;2.
[38] J. B. Wright, "Fracture systems in Nigeria and initiation of fracture zones in the South Atlantic," *Tectonophysics*, vol. 34, no. 3–4, pp. T43–T47, 1976. https://doi.org/10.1016/0040-1951(76)90093-7.
[39] G. J. Genik, "Regional framework, structural and petroleum aspects of rift basins in Niger, Chad and the Central African Republic (CAR)," *Tectonophysics*, vol. 213, no. 1–2, pp. 169–185, 1992. https://doi.org/10.1016/0040-1951(92)90257-7.
[40] A. B. Reid, J. M. Allsop, H. Granser, A. t Millett, and I. W. Somerton, "Magnetic interpretation in three dimensions using Euler deconvolution," *Geophysics*, vol. 55, no. 1, pp. 80–91, 1990. https://doi.org/10.1190/1.1442774.
[41] S. Kasidi and L. G. Ndatuwong, "Spectral analysis of aeromagnetic data over Longuda plateau and environs, North-Eastern Nigeria," *Cont. J. Earth Sci.*, vol. 3, pp. 28–32, 2008.
[42] J. K. Ogunmola, E. A. Ayolabi, and S. B. Olobaniyi, "Structural-depth analysis of the Yola Arm of the Upper Benue Trough of Nigeria using high-resolution aeromagnetic data," *J. Afr. Earth Sci.*, vol. 124, pp. 32–43, 2016. https://doi.org/10.1016/j.jafrearsci.2016.09.008.